Electronic Supplementary Material (ESI) for RSC Advances.


# Supporting Information - Delamination of Graphite in a high pressure homogenizer

Thomas J. Nacken[1], Cornelia Damm[1], Johannes Walter[1], Andreas Rüger[1],Wolfgang Peukert[1]*

[1]Institute of Particle Technology (LFG), Friedrich-Alexander University Erlangen-Nürnberg (FAU), Cauerstrasse 4, 91058 Erlangen, Germany

* Corresponding author Tel: +49 9131-85-29401 E-mail: wolfgang.peukert@fau.de (W.P.)

## Explanation of "cut size"

The cut size corresponds to the maximum diameter of a volume based sphere of graphite, which remains dispersed after a centrifugation run. Equation (I) is derived from Stokes-law for laminar sedimentation of particles in a surrounding liquid phase, including the dynamic viscosity ($\eta$) of the liquid, density of the particles ($\rho_P$), density of the liquid ($\rho_l$), rotational speed ($\omega$), time of centrifugation (t) and the maximum ($r_2$) and minimum ($r_1$) radius of the sample placed in the rotor.

$$cut\ size = \sqrt{\frac{18 \times \eta}{(\rho_p - \rho_l) \times \omega^2 \times t} \times ln(\frac{r_2}{r_1})} \quad \text{(I)}$$

Values used for calculation are presented in table 1.The time was kept constant at 5 minutes for every performed centrifugation run, ω was adapted accordingly. As all suspensions contained a minimum of 98.5 wt.% of water, for the liquid density and viscosity the values for water were used for the calculation.

**Table 1** List of centrifugation related parameters used for cut size calculation.

| Parameter | Value | Comment |
|---|---|---|
| $\eta$ | 1.002 m Pa s | Water at 20 °C |
| $\rho_P$ | 2020 kg $m^{-3}$ | GSI70 feed |
| $\rho_l$ | 998.21 kg $m^{-3}$ | Water at 20 °C |
| $r_2$ / $r_1$ | 0.065 m / 0.021 m | Rotor H12110 |
| $r_2$ / $r_1$ | 0.093 m / 0.031 m | Rotor 19776 |

For centrifugation of the N-methylpyrrolidone (NMP) based suspensions the density and viscosity values of pure NMP (1028 kg/$m^3$ and $1.67 \cdot 10^{-3}$ Pas, respectively) were used for calculation of the cut size.

## Determination of the extinction coefficient

The first important information for any technically relevant production method is the obtained mass of graphene and the related production rate. To calculate the concentration from the UV/Vis-absorbance using the Lambert-Beer law the extinction coefficient for the material must be known. Absorption and scattering of light contribute to the extinction coefficient. In particular the contribution of scattering is a function of particle size and therefore depending on the production process conditions. This is the reason why in literature (for $\lambda$ = 660 nm) different values for the extinction coefficient are found. The values range from 1390-6600 L $g^{-1}$ $m^{-1}$ dependent especially on the product post processing by centrifugation and production method.[4-6] Thus, in the first step it was necessary to determine the extinction coefficient of the dispersed carbon phase for the material prepared by HPH. A standard graphite-water suspension of 5 kg total mass containing GSI70 (1 wt.%) and TW80 (0.5 wt.%) was processed with a nozzle pressure of 40 MPa in batch mode six times. After run 3-6 160 mL of the sample were withdrawn and centrifuged to a cut size of 400 nm. The mass concentration of solid was determined by drying a known volume of the suspension at 90-100°C for 24 hours. After evaporation of the water the residue consisting of residual water, graphene and TW80 was weighted and then transferred into the TGA to determine the exact graphene content (see Figure S2). The extinction coefficient $\varepsilon_C$ was found to be 1028 L $g^{-1}$ $m^{-1}$(±83 L $g^{-1}$ $m^{-1}$) for graphene prepared by graphite delamination by HPH. The number of batch-runs does not have any remarkable influence on the extinction coefficient (see Figure S1).

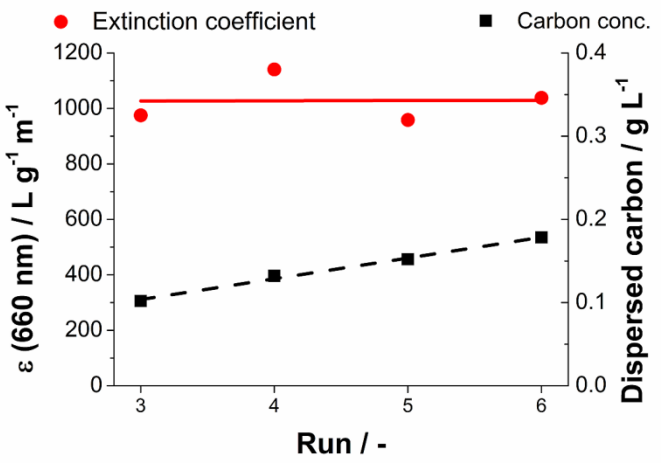


**Figure S1** Obtained dispersed carbon concentration determined by TGA (right axis) and extinction coefficient $\varepsilon_C$ for a suspension of GSI70 (1 wt.%) and TW80 (0.5 wt.%) in water processed with a nozzle pressure of 40 MPa, calculated from the carbon concentration and the absorbance at 660 nm (left axis).

## Thermal gravimetric determination of the Graphite content from a dried processed suspension

The first step of the thermal gravimetric analysis was to distinguish between the adsorbed surfactant and the processed graphite. Reference measurements showed (see Figure S2) that a temperature range exists that can separate the surfactant TW80 and the graphite GSI70. At 450°C, we observed a complete burn-up of TW80 (black line Figure S2 a)), while the mass of GSI70 remained constant at that temperature (red line Figure S2a)). With the temperature rising, GSI70 still showed no weight loss up to 520°C. Above 520°C, GSI70 started to show a slight mass reduction, which continued to become more relevant with increasing temperature. At 1000°C, a complete burn-up of the reference sample of GSI70 could be observed.

Relying on the reference measurements, we were now able to set a temperature range, from 450°C to 1000°C, to differentiate between surfactant and graphite.

When we measured real samples (Figure S2b)), we saw the expected characteristic areas. In order to be sure that no processed graphite is decomposed at temperatures below 520°C, we determined the slope of the TGA-curve between 450°C and 520°C. We obtained values in the magnitude of $10^{-4}$ $K^{-1}$, which indicated no weight loss due to decomposition of carbon in this temperature-range.

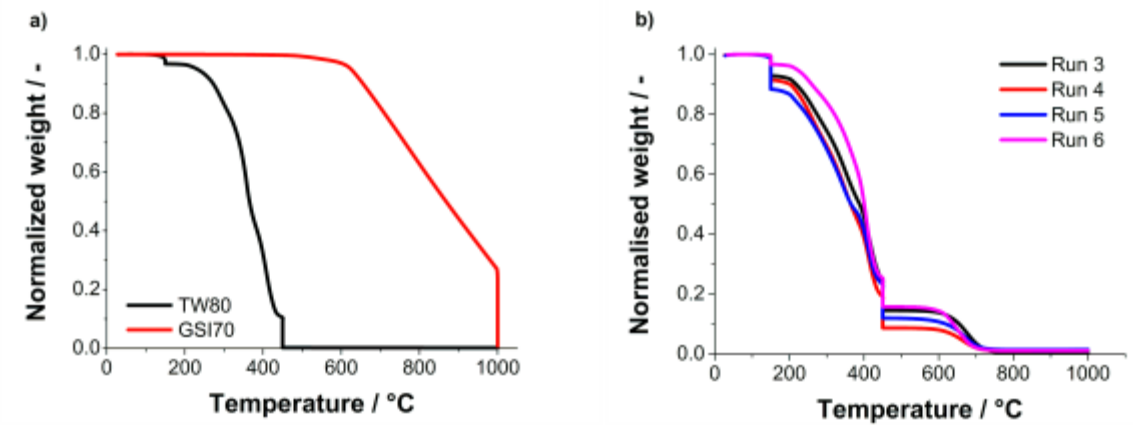


**Figure S2** a) TGA result for a reference sample of GSI70 (red line). For comparison, a TGA graph of a reference sample of TW80 is plotted in the same diagram. For both samples the relative mass over the temperature is shown b) The TGA-results for the real samples processed with 40 MPa nozzle pressure are plotted here as a function of the number of batch runs. The relative sample mass over the temperature, obtained from TGA-measurements, can be observed.

## Impact of cut size to dispersed carbon production

For a cut size of 400 nm a maximum production rate was witnessed for processing with a nozzle pressure of 53 MPa. Applying a second cut size of 200 nm and hence removing all particles above this size, a different picture is generated as ascribed by Figure S 3. In the whole investigated pressure range there is a continuous increase of the dispersed carbon concentration with nozzle pressure (see manuscript). The highest dispersed carbon concentration is observed, as expected, for a nozzle pressure of 70 MPa.

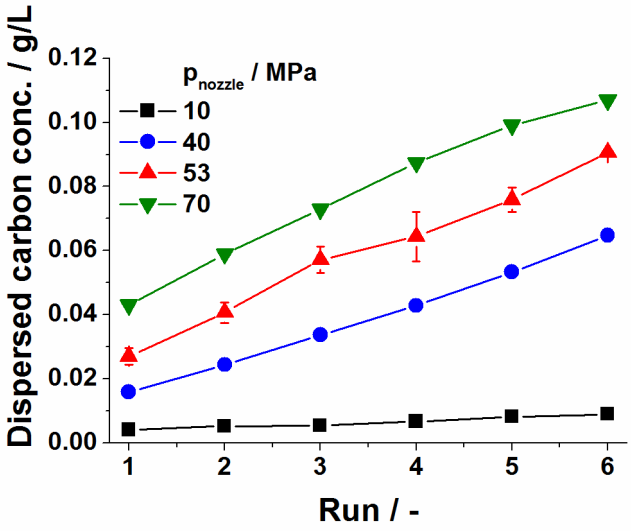


**Figure S 3** Dispersed carbon concentration as a function of performed batch runs for different nozzle pressures for standard suspensions centrifuged to a cut size of 200 nm.

## Influence of formulation on the dispersed carbon concentration

Under optimized processing conditions (nozzle pressure: 53 MPa, no valve pressure) the formulation was varied by changing feed graphite and surfactant, respectively. First the graphite GSI70 was replaced by an unmodified natural graphite (GNP6) and the standard surfactant TW80 was used as stabilizing agent. In a second experiment GSI70 was used in combination with the anionic surfactant sodium dodecyl sulfate (SDS). For both formulations similar production rates are obtained as for the standard formulation, see Figure S4). The slightly increased production rate for GNP6 compared to GSI70 is explained by smaller feed particles, which are easier delaminated.

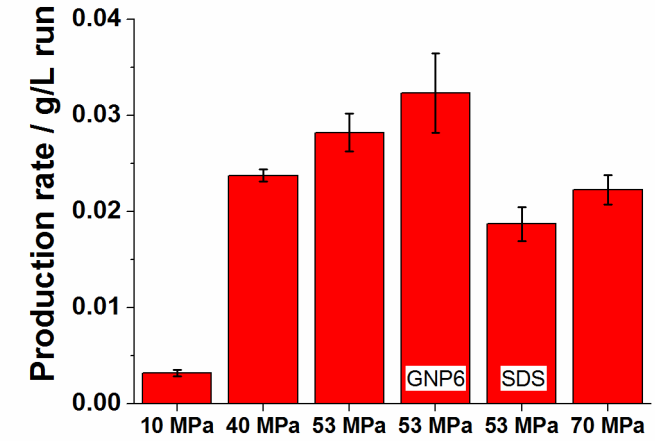


**Figure S 4** Calculated dispersed carbon concentration increase per run for standard suspensions processed at different pressures and for different formulation components processed with 53 MPa (GSI70 + SDS, GNP6 + TW80).

## Raman spectroscopy – graphene related spectra

A selection for typical Graphene spectra obtained via Raman mapping are shown in Figure S5.

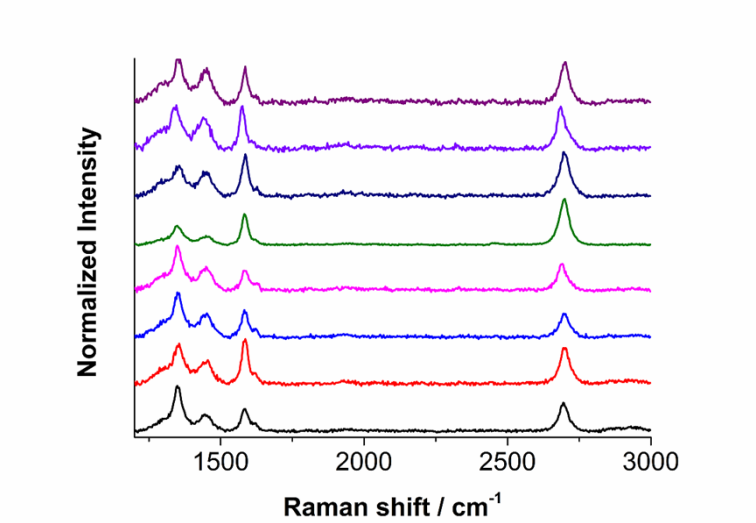


**Figure S5** Typical Raman spectra of graphene (2D-FWHM < 40 $cm^{-1}$) found by Raman mapping for different processed samples.

## Estimation of the Reynolds number

An estimation of the Reynolds number by equation (II) was done for a nozzle diameter D = 240 µm as a function the flow rate which is a function of the nozzle pressure.[1] As can be seen from Figure S5 (left axis) the flow rate is direct proportional to the nozzle pressure.

For the density ρ (in kg/m³) and for the viscosity η (in Pas) the values for water at the temperatures measured for the processed suspensions were used, see table 3.The parameter ν in equation (II) is the flow velocity in m/s which is calculated by relating the flow rate to the nozzle cross-section area.The results in Figure S 6 show, that the Reynolds number is always > 10,000. Thus turbulence is fully evolved at all pressures.

**Table 3** Density ρ and viscosity η of water at the suspension temperatures $\vartheta_s$ measured for the different nozzle pressures $p_{nozzle}$.

| $p_{nozzle}$ / MPa | $\dot{V}$ / L/h | $\vartheta_s$ / °C | ρ / kg/m³ | η / Pas |
|---|---|---|---|---|
| 10 | 20 | 25.7 | 996.94 | $8.72 \cdot 10^{-4}$ |
| 40 | 40 | 33.3 | 994.82 | $7.31 \cdot 10^{-4}$ |
| 53 | 48 | 35.3 | 994.17 | $7.02 \cdot 10^{-4}$ |
| 70 | 60 | 36.1 | 993.91 | $6.92 \cdot 10^{-4}$ |

$$Re = \frac{\rho \cdot D \cdot v}{\eta} \qquad \text{(II)}$$

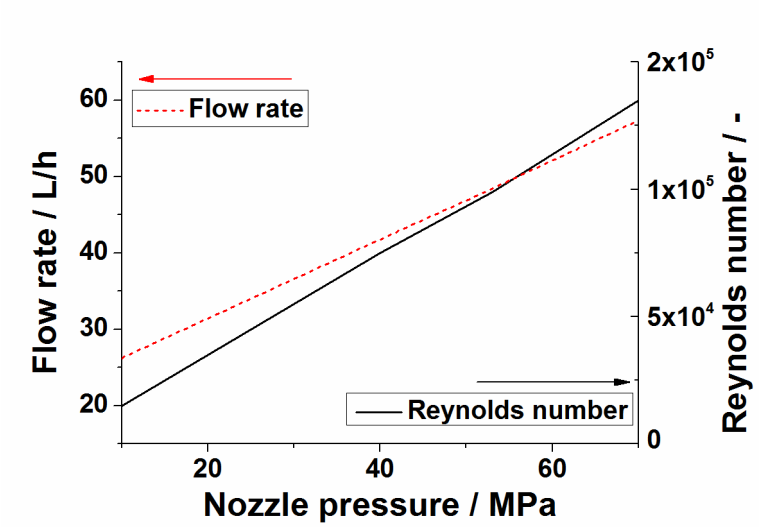


**Figure S 6** Flow rate $\dot{V}$(left axis) and Reynolds number (right axis) created by a pumped suspension through a nozzle 240 µm in diameter.

## Estimation of the role of turbulence-induced particle collisions for graphite delamination by HPH

The probability of graphite delamination by self-lubrication of two colliding graphite feed particles is proportional to the collision kernel $ß_0$ and to the square of the number concentration of feed particles. In all experiments the feed particle concentration is the same. Therefore, the feed particle collision rate increases with growing collision kernel $ß_0$. According to Saffman and Turner the collision kernel between two non-interacting particles in a turbulent flow can be calculated by equation (III) with $x_1$ and $x_2$ diameters of the colliding particles (in m), $E_m$ mass specific energy input (in J/kg), η viscosity (in Pa·s) and ρ fluid density (in kg/m$^3$).[2]

$$ß_0 = \sqrt{\frac{8\pi}{15}} \cdot \left(\left(\frac{x_1}{2}\right) + \left(\frac{x_2}{2}\right)\right)^3 \cdot \left(\frac{E_m \cdot \rho}{\eta}\right)^{1/2} \quad \text{(III)}$$

For HPH the mass specific energy input $E_m$ can be calculated by equation (IV).[3]

$$E_m = \frac{p_{nozzle}}{\rho \cdot c_m} \quad \text{(IV)}$$

$ß_0$ was calculated for $x_1 = x_2 = 20$ µm (mean size of the feed material), for $x_1 = 20$ µm and $x_2 = 200$ nm (example for collision of feed and product particles) and for $x_1 = x_2 = 200$nm (example for collision of two product particles) $c_m = 0.01$ and for the values for $p_{nozzle}$, η and ρ mentioned in table 3.

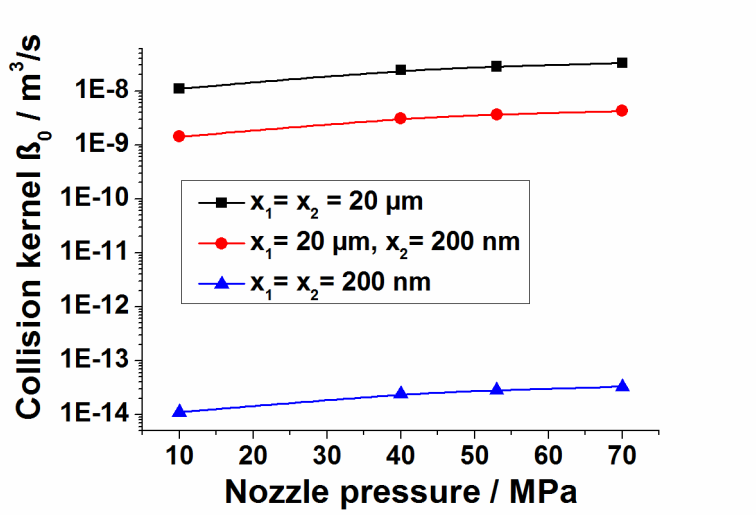


**Figure S 7** Collision kernel $ß_0$ in turbulent flow for two graphite particles with diameters mentioned in the legend.

The results in Figure S7 show that the collision kernel for two feed particles increases about by the factor of 3 if the nozzle pressure increases from 10 MPa to 70 MPa. Thus, for higher nozzle pressure the probability of graphite delamination due to self-lubrication during collision increases.

According to Figure S7 it is expected that the probability of agglomeration also increases with growing nozzle pressure. Moreover, if the number concentrations of feed and product particles are comparable, collisions between feed and product particles are much more frequently than collisions between two product particles as can be concluded from the absolute values of the collision kernel. Thus, collisions between feed and product particles should major contribute to agglomeration.

## Raman and AFM co-localization

The results of statistical Raman spectroscopy and AFM are in excellent agreement with respect to the FLG content. However, as for AFM only small spots on the wafer were measured, results of AFM imaging and Raman mapping may vary depending on the chosen measuring areas. To evaluate precisely the same measuring point in Raman and AFM, both methods have to be co-located. As already mentioned surfactants greatly influence the obtained height by AFM imaging, hence the NMP processed sample used for AFM was also taken for the co-localization. Figure S8 illustrates the evaluated AFM image a) and Raman mapping, respectively b)-d). In total 1173 spectra and 1578 flakes have been evaluated by statistical Raman spectroscopy and AFM imaging, respectively.

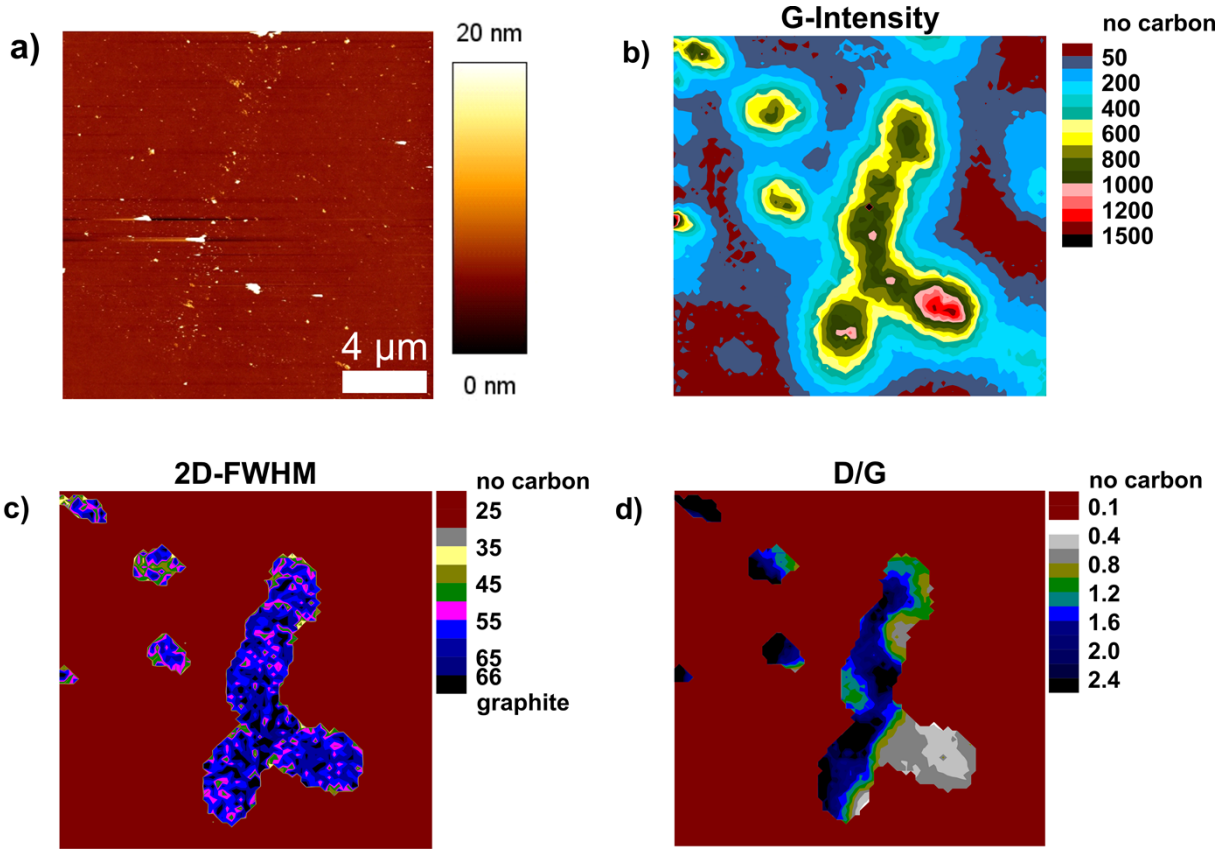


**Figure S8** Co-located NMP processed sample (mapsize 20x20 µm²) a) AFM image with white scale bar of 5 µm, b) intensity map of the G-Raman peak, c) 2D-FWHM map, d) D/G intensity ratio map.

With the mentioned FLG boundary values for Raman (2D-FWHM < 66 $cm^{-1}$) and AFM (flake height < 3.8 nm) we obtained a FLG content for the statistical Raman spectroscopy and for the AFM measurement. While the Raman FLG content derived from the co-located sample (75.7%) is in excellent agreement with the independent Raman spectroscopic and AFM

measurements (FLG 74.4%) and AFM (FLG 75.9%), the co-located AFM measurement suggests a somewhat higher FLG content (86.3%). This is expected as Raman spectroscopy represents a worst case scenario for the FLG content since the 2D-FWHM is broadened by edges and defects. Diameters obtained in co-localization experiments range from 20-480 nm with a mean equivalent disc diameter of 50.1 nm (see Figure S9)).

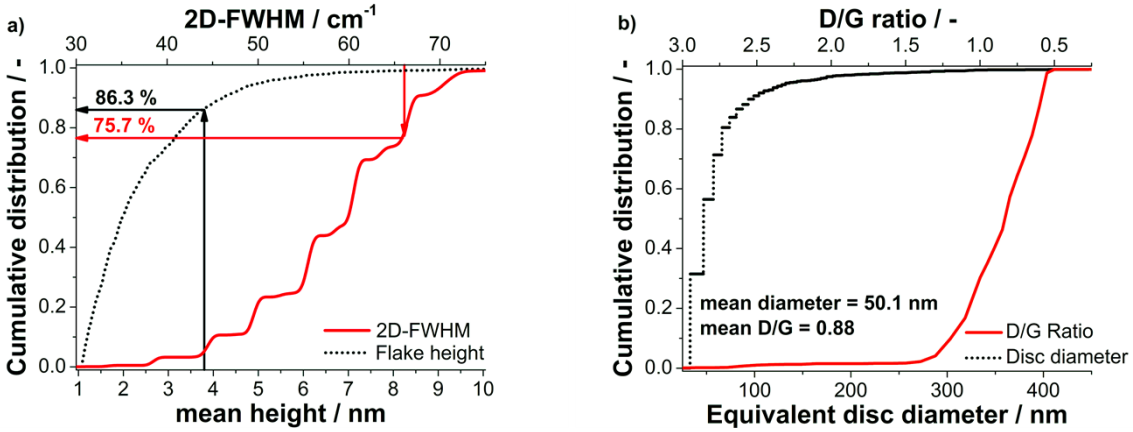


**Figure S9** Cumulative distribution derived from a co-localized sample for statistical Raman spectroscopy and AFM imaging a) 2D-FWHM and mean height b) D/G intensity ratio and equivalent disc diameter.

## References


1 W. Bohl and W. Elmendorf, Stroemungsmaschinen 1: Aufbau und Wirkungsweise, 9th edition, Vogel Business Media, Wuerzburg 2004.

2 P. G. Saffman and J. S. Turner, *J. Fluid. Mech.*, 1956, **1**, 16.

3 K. Köhler (editor) and H. P. Schuchmann, Emulgiertechnik: Grundlagen, Verfahren und Anwendungen, 3rd edition, BEHR'S Verlag, Hamburg 2012.

4 Y. Hernandez, V. Nicolosi, M. Lotya, F. M. Blighe, Z. Sun, S. De et al., Nat. Nano., 2008, 9, 563.

5 M. Lotya, Y. Hernandez, P. J. King, R. J. Smith, V. Nicolosi, L. S. Karlsson et al., J. Am. Chem. Soc., 2009, 10, 3611.

6 M. Yi, Z. Shen, X. Zhang and S. Ma, J. Phys. D: Appl. Phys., 2013, 2, 25301.